JOURNAL OF GEOPHYSICAL RESEARCH: OCEANS, VOL. 118, 166–183, doi:10.1029/2012JC007921, 2013

Impact of tides in a baroclinic circulation model of the Adriatic Sea

A. Guarnieri,[1] N. Pinardi,[2,4] P. Oddo,[1] G. Bortoluzzi,[3] and M. Ravaioli[3]

Received 1 February 2012; revised 8 November 2012; accepted 26 November 2012; published 27 January 2013.

[1] The impact of tides in the circulation of the Adriatic Sea is investigated by means of a nested baroclinic numerical ocean model. Tides are introduced using a modified Flather boundary condition at the open edge of the domain. The results show that tidal amplitudes and phases are reproduced correctly by the baroclinic model and tidal harmonic constants errors are comparable with those resulting from the most consolidated barotropic models. Numerical experiments were conducted to estimate and assess the impact of (i) the modified Flather lateral boundary condition; (ii) tides on temperature, salinity, and stratification structures in the basin; and (iii) tides on mixing and circulation in general. Tides induce a different momentum advective component in the basin, which in turn produces a different distribution of water masses in the basin. Tides impact on mixing and stratification in the River Po region (northwestern Adriatic) and induce semidiurnal fluctuations of salinity and temperature, in all four seasons for the former and summer alone for the latter. A clear presence of internal tides was evidenced in the northern Adriatic Sea basin, corroborating previous findings.

Citation: Guarnieri, A., N. Pinardi, P. Oddo, G. Bortoluzzi, and M. Ravaioli (2013), Impact of tides in a baroclinic circulation model of the Adriatic Sea, *J. Geophys. Res. Oceans*, *118*, 166–183, doi:10.1029/2012JC007921.

1. Introduction

[2] The Adriatic Sea is a semi-enclosed, elongated basin approximately 800 km in length and 200 km in width, exchanging waters with the Ionian Sea and the rest of the Mediterranean at the Strait of Otranto (Figure 1). The bathymetry of the basin is very heterogeneous and can be subdivided into three distinct regions: the northern, central, and southern Adriatic [*Artegiani et al*., 1997a]. The northern part has an average depth of 35 m [*Buljan and Zore-Armanda*, 1976; *Zavatarelli et al*., 2000] and is limited by the 100 m isobath; the central part is characterized by the Pomo Depressions, reaching a maximum depth of about 250 m; the southern part is characterized by the Southern Adriatic Depression (SAD), which is deeper than 1200 m. On the western side the coastal morphology is regular and characterized mainly by sandy beaches, while the eastern side is irregular and characterized by rocky coastlines with a considerable amount of islands.

[3] The basin is characterized by a high freshwater input, due mainly to the River Po (Figure 1), situated in the Italian northwestern coast, and the Buna/Bojana river, a cross-border river between Albania and Montenegro, in the southeastern coast of the basin. Together these two rivers, the mean annual climatological flows of which are 1585 m^3/s [*Raicich*, 1994] and 675 m^3/s [*UNEP*, 1996] respectively, are responsible for almost 40% of the runoff input into the basin, and strongly influence the dynamics of its general circulation.

[4] The two main wind regimes that characterize this region are the Bora and the Sirocco. The former is a very cold, strong, and dry northeasterly wind [*Orlić et al*., 1992], strongly influenced by the orography of the Dinaric Alps, and usually confined to the northernmost part of the basin. The Sirocco is a southerly wind, blowing along the basin's longitudinal axis with the whole basin from southeast to northwest as its fetch, and is thus often partly responsible for high sea levels in the northern Adriatic [*Umgiesser et al*., 2004, *Orlić et al*., 1992].

[5] As far as the basin heat flux budget of the region is concerned, different results have been presented in the literature according to the different periods analyzed and methods used for the analysis. All the different results, though, show negative climatological annual mean heat budgets, varying from –54 Wm^{-2} [*Chiggiato et al*., 2005], to much higher values of about –5 Wm^{-2} [*Maggiore et al*., 1998, *Cardin and Gačić*, 2003]. The most widely accepted values, following *Artegiani et al*. [1997a], range from –22 to –19 Wm^{-2}. On the contrary, recent findings from *Oddo and Guarnieri* [2011] related to the period 2000–2008 propose a very slightly positive general heat budget. The heat budget in the Mediterranean Sea largely depends on the calculation period [*Pettenuzzo et al*., 2010] because winds and air temperatures during winter fluctuate over decadal time scales due to correlation with the North Atlantic Oscillation variability pattern.

[1]Istituto Nazionale di Geofisica e Vulcanologia, Sezione di Bologna, Bologna, Italy.
[2]Department of Physics, University of Bologna, Bologna, Italy.
[3]Consiglio Nazionale delle Ricerche, Istituto di Scienze Marine, Sezione di Geologia Marina.
[4]Centro EuroMediterraneo sui Cambiamenti Climatici, Bologna, Italy.

Corresponding author: A. Guarnieri, Istituto Nazionale di Geofisica e Vulcanologia, Sezione di Bologna, Via D. Creti, 12, 40128 Bologna, Italy. (antonio.guarnieri@bo.ingv.it)

2169-9275/13/2012JC007921

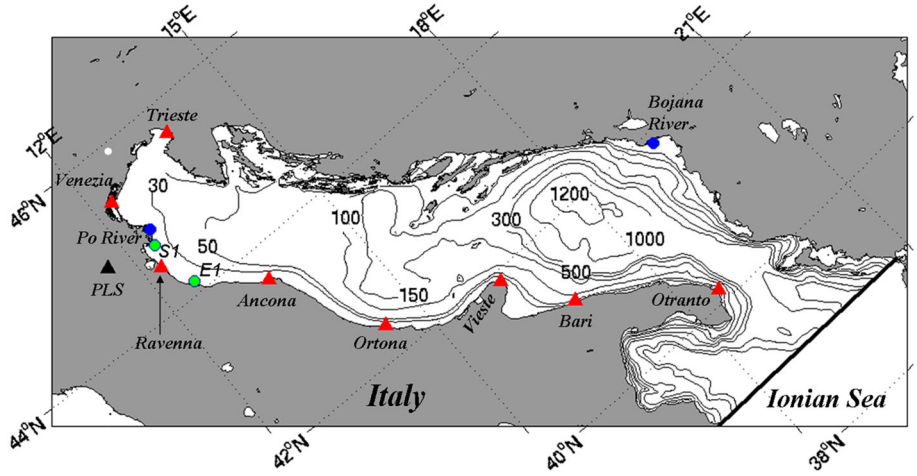

Figure 1. Domain of the Adriatic Sea model. Contour lines represent the bathymetry of the basin; red triangles the locations of Italian tide-gauge stations; green dots the locations of the E1 and S1 multiparameter buoys; blue dots the Po and Buna/Bojana river mouths. The black line across the Ionian Sea represents the model's lateral open boundary.

The combination of the positive water and heat budget gives an overall buoyancy budget, which tends to be very close to zero due to the balancing effects of the water and heat flux components [*Pinardi et al*., 2006].

[6] The forcings and general bathymetry of the basin that have just been described cause the circulation to be generally cyclonic. The main surface circulation features are characterized by a southward current with an observable season-to-season variability—the WACC (Western Adriatic Coastal Current)—along the west coast, which has been divided in the literature into three parts according to their positions (northern, middle, and southern), and by a northward current flowing along the southeastern coast—the Eastern Adriatic Coastal Current—detectable in all the seasons of the year except the summer [*Artegiani et al*., 1997a; *Zavatarelli and Pinardi*, 2003; *Oddo et al*., 2006; *Orlić et al*., 2006]. Besides these currents, three surface cyclonic gyres dominate the northern, middle, and southern basin circulations respectively; these too show an evident seasonal variability, but generally intensify in autumn and, in the case of the southern and central gyres, in summer [*Artegiani et al*., 1997b, *Poulain*, 2001]. The WACC and the Eastern Adriatic Coastal Current interconnect these three gyres with a high intraseasonal variability intensity. As mentioned above, the Adriatic basin exchanges its waters with the rest of the Mediterranean at the Strait of Otranto. Here we have an important inflow of relatively salty and warm waters of Levantine origins at intermediate depths (Levantine Intermediate Waters); these inflow on the Balkan side of the Strait and constitute a heat and salt gain for the basin, acting in competition with the air-sea fluxes and rivers, respectively.

[7] Another important characteristic of the Adriatic general circulation variability at high frequencies is given by astronomical tidal motion. The Adriatic, together with the Strait of Sicily, represents the only area within the Mediterranean where tides have a range of up to more than a meter. These amplitudes occur in the northernmost Adriatic region—the Gulf of Trieste—where the amplitudes of the most energetic frequencies—M2 and K1—reach approximately 27 and 18 cm, respectively. As is known from many studies on barotropic Adriatic tides [*Polli*, 1960; *Zore-Armanda*, 1979; *Mosetti*, 1986; *Malačič et al*., 2000; *Cushman-Roisin and Naimie*, 2002], the diurnal frequencies present weak amplitudes in the southern part of the basin and become enhanced as they move northwards, developing amplitude isolines perpendicular to the longitudinal axis of the basin. The semidiurnal frequencies show an amplitude enhancement in the northern part of the basin with the formation of an amphidromic node [*Polli*, 1960; *Hendershott and Speranza*, 1971; *Mosetti*, 1987; *Tsimplis et al*. 1995; *Cushman-Roisin and Naimie*, 2002] located in the center of the basin, approximately between Ancona (Italy) and Zadar (Croatia) or Sibenik (Croatia), according to the author referred to. According to *Mosetti* [1986], the diurnal and semidiurnal tides are produced by incident and reflected frictionless Kelvin waves, while *Malačič et al*. [2000] interpret the M2 constituent as Kelvin waves propagating along the coasts, as previously found by *Hendershott and Speranza* [1971], and the K1 as continental shelf waves.

[8] The Adriatic tidal regime is not a direct response to astronomical forcing, but is linked to the astronomical tidal oscillations of the Ionian Sea, which induce forced oscillations or seiches of the basin amplified by resonance phenomena along its longitudinal direction from south to north.

[9] Tidal residual velocities have been computed by *Cushman-Roisin and Naimie* [2002] to be a fraction of a centimeter per second, and 1–3 cm near the Po and the islands of Croatia [*Cushman-Roisin and Naimie*, 2002; *Malačič et al*., 2000]. Tidal currents have also been recently studied by *Book et al*. [2009], who showed how they tend to rotate almost completely in most of the areas of the Northern Adriatic, and how the sea elevations and phases increase northwestward and anticlockwise, respectively; this is more evident for semidiurnal than diurnal tides.

[10] Evidence of diurnal thermocline oscillations driven by tidal flow have been proved by *Mihanović et al*. [2009] in the central part of the basin, in particular during the months of June, July, and August. In spite of this tidal

activity, the most energetic driver of the vertical isotherm oscillations for this area turned out to be diurnal wind variability, responsible for oscillations of up to 18 m; twice as much as those due to tides. *Malačič et al*. [2000] studied tidal mixing efficiency, arguing that in the northern region of the basin tides are too weak to mix the water column completely.

[11] In section 2 of this paper we present a new methodology for introducing tides into a baroclinic general circulation model of the Adriatic Sea—the Adriatic Regional model (AREG2), while in section 3 we detail the simulation experiments performed. In section 4 we show the validation of the model results with available in situ and remote information and we quantify the importance of tidal barotropic velocity in the formulation of a modified Flather open boundary condition [*Oddo and Pinardi*, 2008], and finally in section 5 we evaluate the impact of tides on basin dynamics. In section 6 we present a summary of the work done and the conclusions. A detailed description of the circulation model is given in Appendix A.

2. The Circulation Model

[12] The circulation model used in this study—AREG2—is an implementation of the Princeton Ocean Model [*Blumberg and Mellor*, 1987] in the Adriatic, and has already been used in the past for modeling studies and operational forecasting with different resolutions [*Zavatarelli et al*., 2002; *Zavatarelli and Pinardi*, 2003; *Oddo et al*., 2005, 2006; *Oddo and Guarnieri*, 2011].

[13] The model domain covers the entire Adriatic Sea (see Figure 1) and presents a lateral open boundary line at 39°N, where it is nested into the operational Mediterranean Forecasting System (MFS) model [*Tonani et al*., 2008; *Pinardi and Coppini*, 2010]. The model's horizontal resolution is approximately 1/45°, and it is implemented on 31 vertical sigma layers, with the topography above 10 m set everywhere to 10 m. The model is forced with analysis fields of the European Centre for Medium-Range Weather Forecast (ECMWF) at a horizontal resolution of 0.5° and the frequency of 6 h (see section A1). Previous modeling work has pointed out that this coarse resolution could imply the loss of some spatial and temporal variability in the currents, especially during the Bora events [*Pullen et al*., 2007]. However, we do not believe that these particular scales affect the present work, which is to study the impact of tides on the circulation of the Adriatic Sea.

[14] The governing equations of the model are reported in Appendix A along with their specific vertical boundary conditions and numerical choices, while here we will limit the discussion to the lateral open boundary conditions with tidal signal.

[15] The approach used to account for lateral forcing of tides in the Adriatic is similar to that used by *Changshui et al*. [2006] and *Xingang et al*. [2010] for the Yellow Sea, but more general. It derives from the formulation by *Flather* [1976] on barotropic velocities at the open boundary line as generalized by *Oddo and Pinardi* [2008]. This defines the boundary conditions for the barotropic normal component as

$$V = \frac{H^{\text{nesting}} + \eta^{\text{nesting}}}{H + \eta} V^{\text{nesting}} - \frac{C}{H + \eta}\left(\eta^{\text{nesting}} - \eta\right) \tag{1a}$$

where the variables without superscripts refer to the nested model and the barotropic velocity component normal to the boundary section. In our case, at the open boundary section, the two bathymetries coincide, i.e., $H^{\text{nesting}} = H$, and assuming that $H \gg (|\eta^{\text{nesting}}|, |\eta|)$ and the wave phase speed $C = \sqrt{gH}$, with g the gravitational acceleration, we obtain

$$V = V^{\text{nesting}} - \frac{\sqrt{gH}}{H}\left(\eta^{\text{nesting}} - \eta\right). \tag{1b}$$

[16] In our case we want to use the barotropic velocity from the MFS model with the addition of the astronomical tidal signal, as derived from a separate tidal model. Thus, $V^{\text{nesting}} = V^{\text{MFS}} + V^{\text{tides}}$, and $\eta^{\text{nesting}} = \eta^{\text{MFS}} + a\eta^{\text{tides}}$ where a is a calibration constant introduced following underestimation of tidal amplitude in the northernmost part of the basin when integrating the model in barotropic mode. Its value after calibration resulted as $a = 1.1$.

[17] This linear superposition of the signals is commonly assumed for other different semi-enclosed or totally open shelf areas.

[18] *Changshui et al*. [2006] and *Xingang et al*. [2010] omitted the tidal barotropic velocity (V^{tide}) in their formulation of equation (1b). We will show in this study (section 4.3) that in spite of its small amplitude, this term is rather important for the correct evaluation of the tidal harmonic constants around the basin, at least in the case of the Adriatic.

[19] The open boundary tidal elevations and velocities are obtained from the OTPS tidal model (*Oregon State University Tidal Prediction Software*: http://volkov.oce.orst.edu/tides/otps.html, *Egbert and Erofeeva* [2002]) provided on a regular lon/lat grid at a horizontal resolution of 1/12 of a degree. The constituents used to evaluate the tidal elevation and normal velocity at the boundary line were the eight most significant ones: M2, S2, N2, K2, K1, O1, P1, Q1.

[20] To conserve the net barotropic transport from MFS across the open boundary, the integral constraint of *Pinardi et al*. [2003] was imposed. If we define $V^{\text{MFS}}_{\text{orig}}$ as the normal barotropic velocity to the boundary line and $V^{\text{MFS}}_{\text{int}}$ as its interpolation on the nested model grid, the transports M_{orig} and M_{int} across the nesting line are

$$M_{\text{orig}} = \int_{x_2}^{x_1} \int_{-H_{\text{nesting}}}^{\eta_{\text{nesting}}} V^{\text{MFS}}_{\text{orig}}(x, y, z, t)\, dz dx, \tag{2}$$

and

$$M_{\text{int}} = \int_{x_2}^{x_1} \int_{-H}^{\eta} V^{\text{MFS}}_{\text{int}}(x, y, z, t)\, dz dx, \tag{3}$$

where x_1 and x_2 are the longitudinal limits of the open boundary section that are identical in the two models. If we define $\Delta M = M_{\text{int}} - M_{\text{orig}}$ the difference in transport only due to interpolation and $S = \int_{x_2}^{x_1} \int_{-H}^{\eta} dz dx$, we assume a correction to the MFS velocity field as

$$V^{\text{MFS}}_{\text{corr}} = \Delta M / S, \tag{4}$$

Table 1. Simulation Experiment Acronyms: The Simulations Differ According to Whether Tides Are Included and the Type of Lateral Boundary Conditions Used

Experiment Name	Tides	Lateral Boundary Condition
INT1	Yes	$V = \left(V^{\mathrm{MFS}} + V^{\mathrm{tides}}\right) - \frac{\sqrt{gH}}{H}\left(\eta^{\mathrm{MFS}} + a\eta^{\mathrm{tides}} - \eta\right)$
INT2	Yes	$V = V^{\mathrm{MFS}} - \frac{\sqrt{gH}}{H}\left(\eta^{\mathrm{MFS}} + a\eta^{\mathrm{tides}} - \eta\right)$
INT3	No	$V = V^{\mathrm{MFS}} - \frac{\sqrt{gH}}{H}\left(\eta^{\mathrm{MFS}} - \eta\right)$

so that the original transport is maintained. The resulting total velocity of the nested model along the open boundary will then be

$$V^{\mathrm{nesting}} = V^{\mathrm{MFS}}_{\mathrm{int}} - V^{\mathrm{MFS}}_{\mathrm{corr}} + V^{\mathrm{tides}}. \tag{5}$$

3. Simulation Experiments

[21] The model described in section 2 was used to carry out 9 year simulations from January 2000 to December 2008. The main aim of the simulations is twofold: first to evaluate the quality of a baroclinic tidal model simulation with respect to consolidated barotropic simulations of the Adriatic Sea [*Cushman-Roisin and Naimie*, 2002; *Bellafiore et al*., 2008], and second, to show the dynamical effects of tidal motion on baroclinic circulation.

[22] In experiment INT1 (see Table 1), the model was initialized in January 2000 from a previous integration of the same circulation model without tides [*Guarnieri et al*., 2010], and tides were introduced with the full lateral boundary condition formulation. To estimate the importance of the tidal barotropic velocity in the formulation of the lateral boundary condition, experiment INT2 (Table 1) did not consider the tidal barotropic velocity term V^{tide} in (1b). Lastly, to investigate the impact of tides on the dynamics of the basin, experiment INT3 (Table 1) was carried out, removing the tidal forcing completely.

[23] In the following sections, we first discuss the validation of the simulated tidal motion and the thermodynamics fields, then discuss the importance of tidal lateral boundary conditions, and finish by discussing the importance of tidal motion on the basin circulation structure and dynamics.

4. Validation of the Baroclinic Ocean Model With Tidal Components

4.1. Tidal Components and Sea Level

[24] Here we show that a conventional baroclinic general circulation model can reproduce standard barotropic tidal model results for the Adriatic.

[25] The tidal phases and amplitudes resulting from INT1 were estimated through a harmonic analysis of the sea surface elevation on an hourly basis using the methodology of *Pawlowicz et al*. [2002] at each grid point of the model for the year 2003. The results for the most important semidiurnal and diurnal constituents (M2, S2, K1, O1) are presented in the left-hand panels of Figure 2, where the cotidal lines are thinner and the corange lines thicker. The right-hand panels of the figure are the results from a consolidated barotropic model by *Cushman-Roisin and Naimie* [2002], here considered our reference model.

[26] The figure shows that AREG2 is capable of reproducing most of the features of the diurnal and semidiurnal tidal constituents, in terms of both amplitude and phase.

[27] The semidiurnal tidal constituents M2 and S2 resulting from the simulation from AREG2 are overestimated in terms of amplitude compared to the results achieved by *Cushman-Roisin and Naimie* [2002], which underestimate, however, the observed values of amplitude for the M2 constituent. On the other hand, AREG2 K1 and O1 diurnals in the northernmost side of the basin are underestimated by approximately 2.5 and 1.5 cm, respectively.

[28] The same type of analysis was carried out comparing the model harmonic constants with those derived from various Italian tide-gauge stations. The locations of the stations are shown in Figure 1 (red triangles). The comparison between the model and the observations is presented in Table 2 for the period February 2000 to December 2008. The top half of Table 2 refers to the tide amplitude and the bottom half to the tide phase lag with respect to the local time (UTC+1). For each constituent the corresponding left-hand column of the table shows the results of observations, the central column shows the results of AREG2 simulations and the right-hand one shows the percentage error. The error was calculated for amplitude and phase respectively, as follows:

$$E^{\mathrm{amp}}_{\%} = \left|\frac{A^o - A^m}{A^o}\right| \times 100, \tag{6}$$

$$E^{\mathrm{pha}}_{\%} = \left|\frac{P^o - P^m}{180}\right| \times 100, \tag{7}$$

where A and P are the tidal amplitude and phase and the superscripts "o" and "m" refer to observations and model, respectively. This means that the error in phase is 100% when the modeled phase has the opposite direction to the observations.

[29] The main errors are related to the diurnal constituents, in both amplitude and phase, and O1 in particular. As recalled by *Cushman-Roisin and Naimie* [2002], the estimate of the phase of this constituent has always been problematic, and the literature shows very different values at all stations. For example, in Trieste it ranges from 39° [*Tsimplis et al*., 1995] to 62° [*Polli*, 1960]. Our model yields 39°, in agreement with *Tsimplis et al*. [1995], but the phase that we estimate from observations is 58°, evidencing an 11% discrepancy (calculated according to equation (7)). As far as amplitude is concerned, the most problematic constituent is once again O1 in percentage terms: error versus observations reaches 25%. As described in section A1, the numerical model used in the present simulations was forced with ECMWF atmospheric forcings at 0.5° of resolution and 6 h of frequency. As proved by *Orlić et al*. [2011] the diurnal breezes in the Adriatic Sea may have a very strong impact on diurnal variations in the flow field superimposed on tidal oscillations, and thus affect these latter. A possible explanation to the fact that the diurnal constituents are affected by relatively larger errors might then be related to the inability of the model to capture wind-related processes mainly on diurnal frequencies—such as the summer sea breeze cycle [*Orlić et al*., 2011], which may interact with the tidal amplitude oscillations and phases. The best result in amplitude is

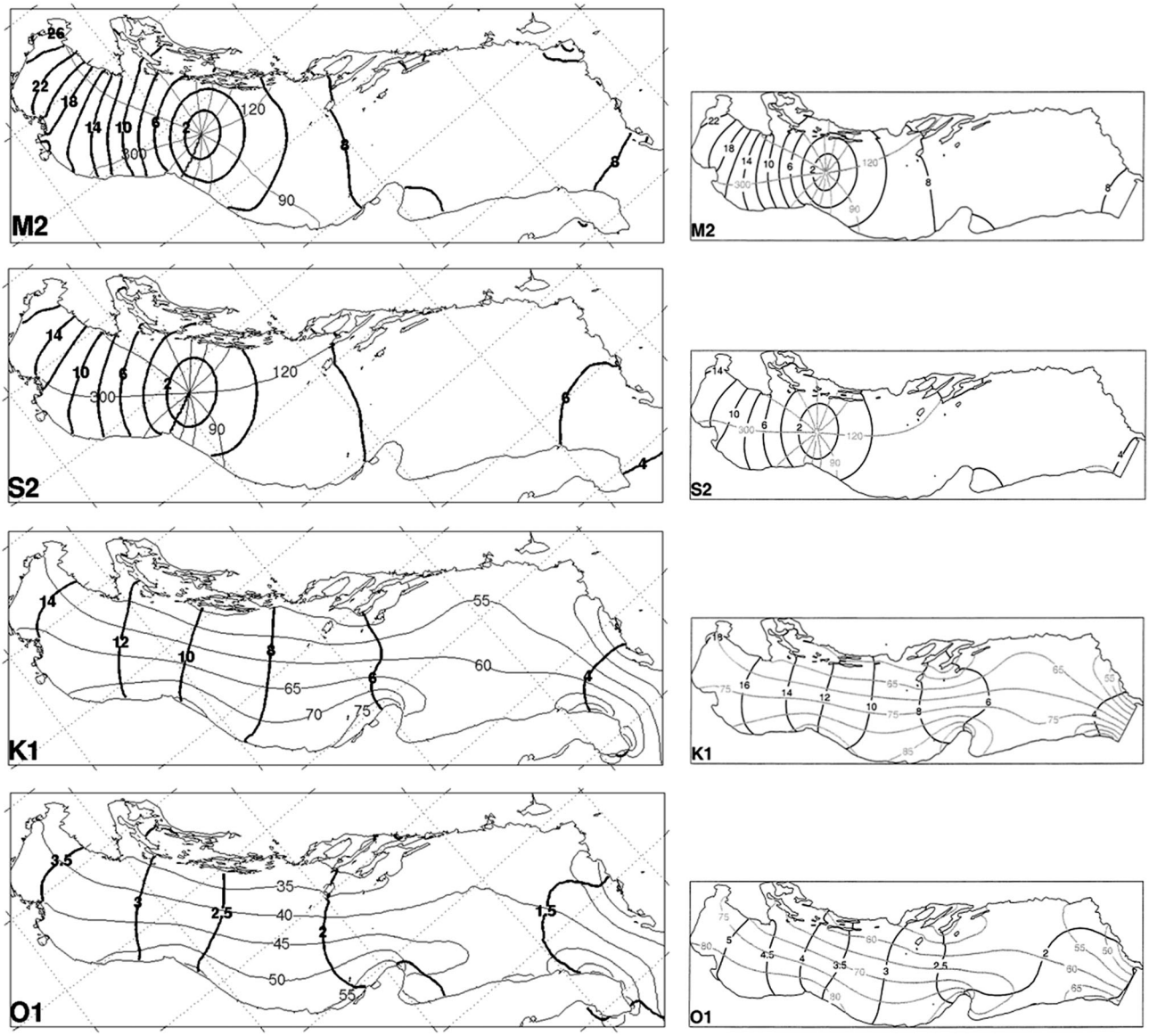

Figure 2. Amplitude and phase distribution of the M2, S2, K1, and O1 tidal constituents reproduced with the baroclinic model described in the present work (left) and with the barotropic model described by *Cushman-Roisin and Naimie* [2002] (right).

achieved for the reproduction of the most energetic frequency, M2, with an average error around the basin of only 2%.

[30] The tidal components were also assessed for the currents measured at the E1 buoy (see Figure 1 for the location of the buoy) [*Russo et al*., 2009]. Table 3 shows the comparison between observed and modeled data in terms of major and minor tidal ellipse axes and orientation for a period of 48 days. The modeled reproduction of the major axis of the tidal ellipses is accurate, but generally underestimated, while the minor axis is overestimated for the semidiurnal components and underestimated for the diurnal K1 constituent. In Figures 3a and 3b a comparison between the current tidal components at 8.5 m is shown from 20 November to 5 December 2006 at the E1 location. The hourly total currents of Figures 3c and 3d show how the total current is generally reproduced well by the model, even though the amplitude of the highest and lowest peaks is usually underestimated. The model also fails in the reproduction of the very sudden and strong variability of the current signal. As evidenced by *Orlić et al*. [1994] and by *Poulain et al*. [2004] under particularly strong Sirocco conditions, the dominant southward WACC may reverse in direction. This happens when the buoyancy-driven residual flow becomes weaker than the wind-induced current component, favoring water piling up in the North Adriatic with possible flood events. During the analyzed period, only on 9 December 2006 the wind forcing presents an evident footprint of Sirocco, which results in a significant reversal of the WACC lasting for a couple of days, as visible in the Figure 3d. This

Table 2. Tidal Amplitudes and Tidal Phase Lags With Respect to the Local Time (UTC+1)[a]

	M2			N2			S2			K2			O1			P1			K1			AVERAGE
Station	obs	mod	Diff %	obs	mod	Diff %	obs	mod	Diff %	obs	mod	Diff %	obs	mod	Diff %	obs	mod	Diff %	obs	mod	Diff %	DIFFERENCE %
Amplitudes (meters)																						
Ancona	0.067	0.067	0	0.012	0.012	3	0.036	0.040	10	0.011	0.012	8	0.042	0.030	28	0.045	0.037	19	0.135	0.111	18	12
Bari	0.097	0.098	1	0.015	0.016	7	0.060	0.065	9	0.017	0.019	13	0.019	0.016	16	0.018	0.016	12	0.052	0.049	5	9
Ortona	0.069	0.065	6	0.012	0.010	11	0.048	0.050	3	0.015	0.015	2	0.030	0.022	26	0.031	0.026	17	0.092	0.078	15	11
Otranto	0.070	0.075	8	0.012	0.013	10	0.041	0.046	13	0.011	0.013	19	0.009	0.011	17	0.010	0.010	3	0.024	0.030	24	13
Ravenna	0.169	0.169	1	0.029	0.029	1	0.100	0.110	10	0.030	0.032	7	0.051	0.034	33	0.055	0.044	20	0.166	0.135	19	13
Trieste	0.267	0.263	1	0.045	0.052	17	0.160	0.177	10	0.048	0.052	8	0.053	0.037	31	0.063	0.048	23	0.182	0.149	18	15
Venezia	0.241	0.238	1	0.041	0.040	2	0.143	0.158	10	0.044	0.046	6	0.054	0.036	33	0.060	0.047	21	0.181	0.145	20	13
Vieste	0.095	0.097	2	0.016	0.016	0	0.061	0.066	9	0.017	0.020	13	0.018	0.015	19	0.020	0.016	20	0.053	0.048	11	10
AVERAGE DIFFERENCE %			2			6			9			10			25			17			16	12
Phases (degrees)																						
Ancona	330	321	5	332	321	6	344	340	2	341	338	2	71	54	10	80	71	5	87	74	7	5
Bari	112	100	7	110	102	5	120	111	5	115	108	4	56	42	8	63	60	2	72	61	6	5
Ortona	93	86	4	90	85	3	101	101	0	95	97	1	68	52	9	78	69	5	83	72	6	4
Otranto	105	102	2	102	103	0	112	114	1	109	111	1	62	46	9	71	59	7	75	63	7	4
Ravenna	302	295	4	302	296	3	310	307	2	306	304	1	67	47	11	78	65	7	83	69	8	5
Trieste	278	273	3	278	275	2	287	284	2	283	281	1	58	39	11	65	56	5	71	59	7	4
Venezia	287	283	3	287	284	1	295	295	0	291	292	0	61	42	10	70	61	5	77	64	7	4
Vieste	102	97	3	102	98	2	111	110	1	105	106	0	77	57	11	84	75	5	91	78	7	4
AVERAGE DIFFERENCE %			4			3			2			1			10			5			7	4

[a]For each constituent the corresponding left-hand columns of the tables show the results of observations, the central columns the results of AREG2 simulations, while the right-hand columns show the absolute value of the percentage error.

Table 3. Observed and Modeled Tidal Ellipses at the E1 Buoy for a Depth of 8.5 m. The Analysis Was Performed on a 48 Day Long Interval, From 1 November to 19 December 2006

E1 Station (Lon=12°34.219' Lat=44°08.599')						
	Major Axis (cm/s)		Minor Axis (cm/s)		Orientation (°)	
Constituent	OBS	MOD	OBS	MOD	OBS	MOD
M2	4.0	3.7	0.5	1.0	-49	-46
S2	2.5	2.3	0.1	0.4	-58	-51
K1	2.0	1.8	0.6	0.3	-10	-3

Table 4. Mean Errors for the Sea Surface Elevation for the INT1 Simulation. The Analysis Was Performed in the Interval Between February 2000 and December 2008

Elevation Mean Errors (cm)			
Station	RMSE	Station	RMSE
Ancona	8	Ravenna	8
Bari	6	Trieste	9
Ortona	7	Venezia	9
Otranto	6	Vieste	6
Mean root-mean-square error (RMSE) = 7 cm.			

is probably also favored by the low Po River flow, which is below the annual average value, thus contributing to keep the buoyancy forcing low.

[31] A comparison between modeled total sea level and sea level as observed with tide gauges is, to the best of our knowledge, something never offered for the Adriatic. In fact, both the tidal and storm surge models are usually barotropic, and thus do not account for the variation of the sea level due to baroclinic processes.

[32] The baroclinic induced sea level, normally described by the dynamic height or topography, has frequencies in the order of days, months, and even years, while the barotropic sea level variations might have higher frequencies, in the order of hours. The sea level changes due to baroclinic processes are in the order of a few centimeters, which is comparable to the sea level error of the model, as shown in Table 4. Therefore, we believe that it is very important for an ocean model to account for this part of the signal, which is inevitably not accounted for in a barotropic model.

[33] Figure 4 shows the comparison between the modeled sea surface height (SSH) in the baroclinic integration INT1 and the observed height at the tide-gauge stations mentioned above (see Table 2 and Figure 1).

[34] The first and third panels of Figure 4 show the comparison for the tide gauge in Trieste for a 2 week period during April and September 2008, and the second and last ones represent the comparison in Ravenna for the same period. Because the model and the tide gauge station values have different reference systems, an SSH anomaly has been defined by subtracting the mean value of each data set at the stations. The observed and modeled mean SSH values for Trieste in the aforementioned period are 7 and –9 cm, respectively. For Ravenna they are 4 and –5 cm. Table 4 shows the root-mean-square error of the modeled SSH anomaly with respect to the observations for the analyzed stations. The error, calculated for the period 2000–2008 on 1 h frequency data, ranges between 6 and 9 cm, and has a mean value around the basin of approximately 7 cm. The error in the reproduction of the SSH anomaly can be due partly to the missing astronomical components (all the frequencies lower than the diurnal are missing), partly to model errors, mostly related to the inaccurate knowledge of the model coastlines and bathymetry, and the absence of atmospheric pressure in the model. However, we argue that the Adriatic baroclinic tidal model shown here is comparable to any barotropic tidal model used in the past.

4.2. Validation of the Model Temperature and Salinity

[35] The daily mean simulated temperature and salinity from INT1 were compared to approximately 2400 available

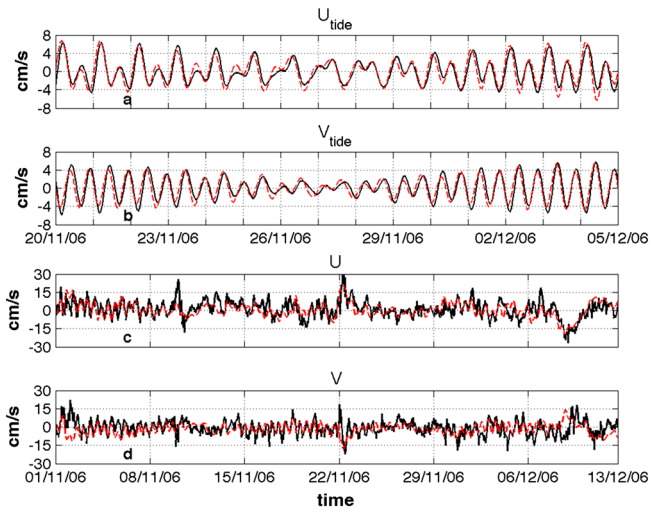

Figure 3. Validation of the bottom tidal components of the currents at the E1 buoy station ((a) zonal and (b) meridional) and of the bottom full currents ((c) zonal and (d) meridional). The black solid line represents observations; the dashed red line model simulations.

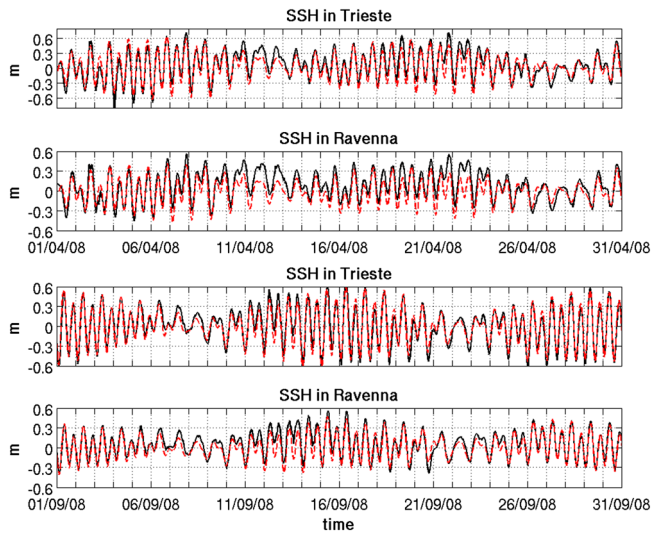

Figure 4. Comparison between modeled INT1 SSH (dashed red line) and observed SSH (solid black line) at the Italian tide-gauge stations of Trieste (first and third panels) and Ravenna (second and fourth panels). The two data sets are on an hourly basis.

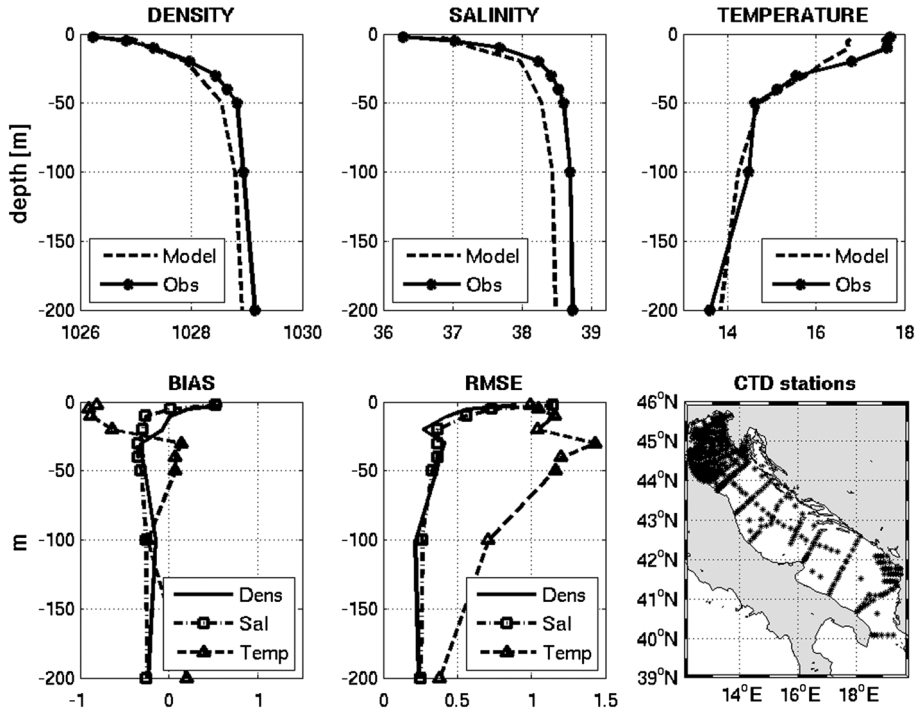

Figure 5. Model validation. In the top panels the mean observed (solid line) and simulated (dashed line) profiles of density, salinity and temperature are presented. In the bottom panels the bias and root-mean-square error of the same variables are presented (left and middle panels, respectively). The profiles are averaged over space and time. The black stars of the bottom-right panel represent the locations of the stations. The simulated data are daily means.

CTD profiles sampled during the period 2001–2008. The station locations are represented by the black stars in the map at the bottom of Figure 5, and mean profiles (averaged in time and space), biases (model-observations) and root mean square errors are presented for density, salinity, and temperature. The simulated profile structure fits fairly well with observations, but significant biases occur, such as the deep salinity freshening. In particular, the model tends to be colder than observations in the first 20 m, while model salinity is about 0.25 practical salinity unit (PSU) lower than observations. Furthermore, the simulated mixed layer depth is too diffuse, which may be due to the *Mellor and Yamada* [1982] vertical mixing scheme, which tends to overmix.

[36] The basin mean sea surface temperature (SST) compared to satellite gridded data [*Sciarra et al.*, 2006], presents a bias of approximately 0.8°C averaged over the years (not shown), and a root mean square error of approximately 1.3°C (not shown). Figure 6 shows the modeled (dashed red line) and observed (solid black line) monthly mean sea surface temperature in the top panel and the related anomaly in the bottom panel. The SST dynamics are represented well by the model, which is able to reproduce the interannual and intra-annual variability well, and presents a Nash-Sutcliff efficiency [*Nash and Sutcliffe*, 1970] of approximately 0.96 on the full signal, which decreases to approximately 0.67 after removing the monthly climatology. It is clear that the model presents a negative bias, which is usually enhanced during late spring (June) and early summer (July and August). The main differences in the anomalies between the model and the observations are recorded in 2004, when the modeled SST seems to be slightly out of phase compared to the observations, and thus not able to reproduce the negative anomaly of the first part of this year. In the middle part of 2007 we also highlight relevant differences between the observed and the modeled anomalies. In this case, the model is always colder than the satellite observations, and is unable to reproduce the correct intensity of the SST anomaly, even though the trend of the curve is well represented.

[37] It should be noted that the model grid points where the first sigma layer is deeper than 1.5 m have not been used

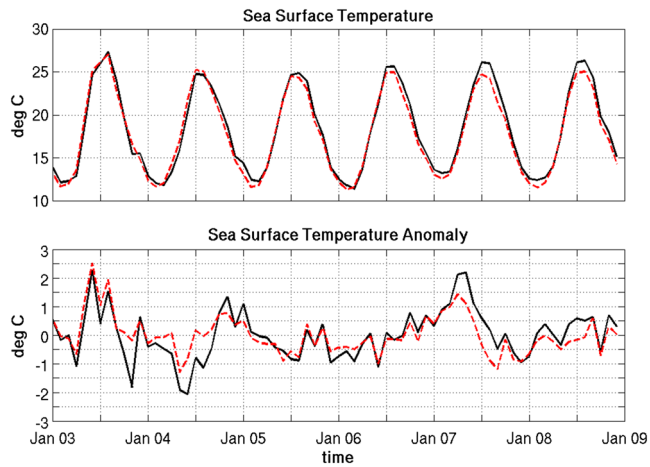

Figure 6. Validation of SST and SST anomaly for the period 2003–2008. (top) Monthly means of sea surface temperature from the satellite (black solid line) and from the model (red dashed line). (bottom) Anomalies.

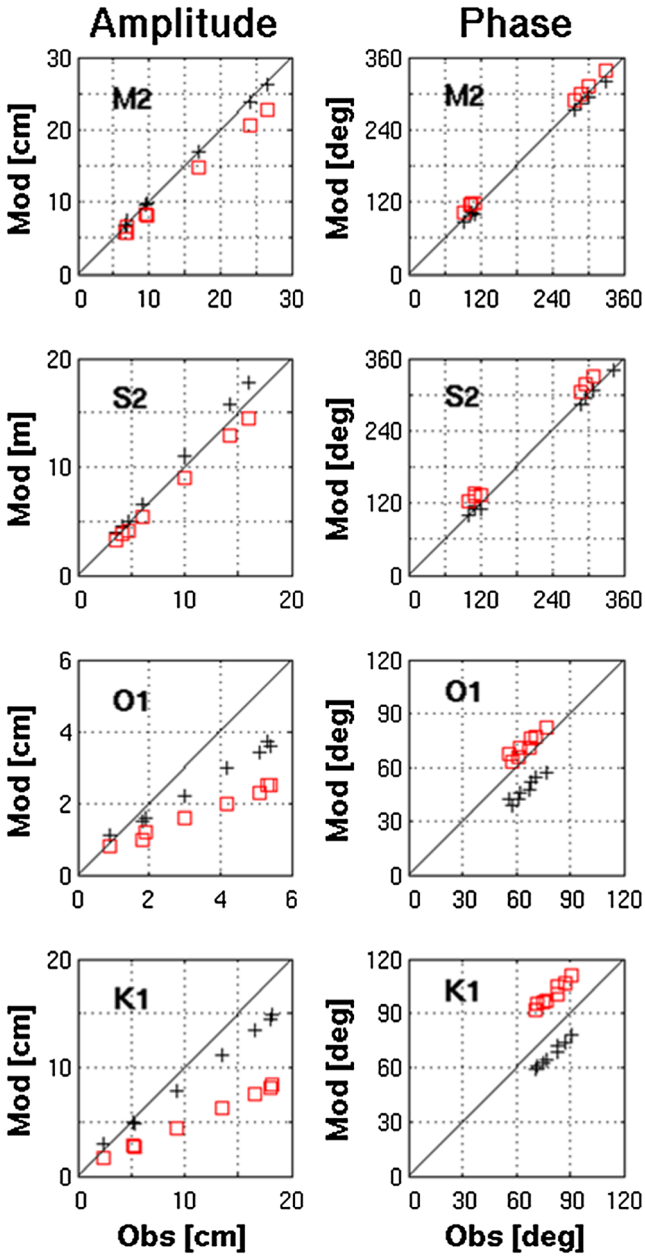

Figure 7. Validation of the amplitude and phase of M2, S2, O1, and K1 tidal constituents for integrations INT1 (black crosses) and INT2 (red squares). The harmonic analysis was assessed for a 1 year period. Observations are on the x axis and simulations on the y axis.

for the SST intercomparison and a threshold of at least 1000 grid points in the satellite observations has been used, under which the data were not considered for intercomparison.

4.3. Influence of Open Boundary Condition Formulation

[38] Experiment INT2 (Table 1) allowed estimating the importance of the tidal barotropic velocity component (V^{tides}) in the formulation of the open lateral boundary condition (equation (1b)). This integration was carried out from the beginning of December 2002 to the end of December 2003. The first month of simulation was not used for the tidal analysis performed.

[39] The results of the harmonic analysis of the INT2 sea surface height in terms of amplitude and phase were compared to INT1. The comparison of the two datasets is shown in Figure 7 for the two most energetic diurnal and semidiurnal constituents: M2, S2, O1, K1. The semidiurnal frequencies are represented well by the INT1 model, in terms of both amplitude and phase, and the improvement due to the barotropic velocity term in the open boundary condition is evident. The reproduction of the diurnal frequencies (O1 and K1) is not as accurate as for the semidiurnal ones, but once again the improvement due to the addition of the barotropic velocity term is evident, mainly in terms of amplitude. The only exception to the improvement of INT1 with respect to INT2 is for the O1 phases.

[40] In general, we conclude that the barotropic velocity term in the open boundary condition has a positive impact on the reproduction of the basin tidal signal. For the diurnal constituents it can be responsible for up to 50% of the single amplitude signal simulated (this is the case of K1 amplitude), while the influence in the phase lag appears to be much more confined (no higher than 11%, S2 and K1 constituents).

5. Impact of Tides on Adriatic Sea Dynamics

[41] To evaluate the impact of tides on the system dynamics, a third simulation (INT3, see Table 1) was carried out, removing the tidal forcing completely. INT3 was initialized with a snapshot of INT1 in January 2005 and run up to December 2006. The first year of integration was considered a spin-up and only the results for 2006 are discussed.

5.1. Effect of Tides on Temperature and Salinity

[42] Figure 8 shows the anomalies of temperature and salinity at the S1 and E1 buoys (Figure 1) [*Bortoluzzi et al.*, 2006] for the periods 1 July to 1 October 2006 for S1, and 1 November to 30 December 2006 for E1. The data sampled by the buoys are at the depth of approximately 1.2 m at S1 and 1.6 m at E1, with a frequency of 1 h. The S1 buoy is located just a few kilometers south of the Po River delta, and is clearly in a region of freshwater influence (ROFI) [*Sanchez-Arcilla and Simpson*, 2002] with a bottom depth of approximately 20.5 m (Figure 1). The E1 buoy is also located just a few kilometers off the coast, in a region still strongly influenced by Po River runoff. Both models, with and without tides, are capable of representing high-frequency daily surface temperature signals due to the daily surface heat cycle. For salinity instead the situation is more complex and there is a large mismatch between model and observations probably due to the fact that both stations are located across the salinity front due to the Po River runoff and thus the uncertainty due to model resolution is maximum.

[43] However, the model with tides is capable of representing a higher frequency variability, as shown in Figure 9, where a zoom of the near-bottom transport of temperature and salinity at buoy E1 is shown. Transports were calculated on hourly data as $Q_x = u_{\text{bot}}X$ for the cross-shore component, and as $Q_y = v_{\text{bot}}X$ for the along-shore component, where u_{bot} and v_{bot} are the near-bottom zonal and meridional components of velocity (m/s) respectively, and X is the state

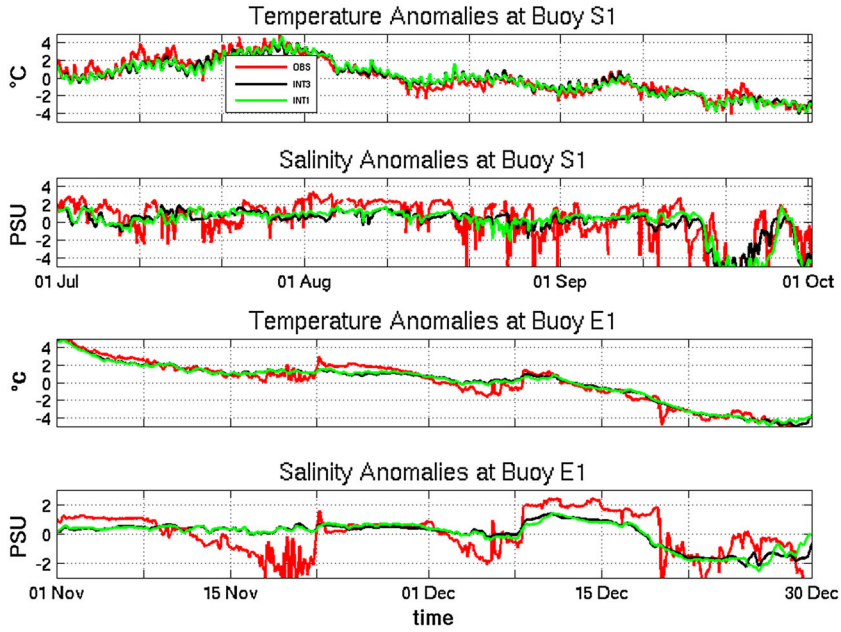

Figure 8. Temperature (°C, first and third panels) and salinity (PSU, second and fourth panels) anomalies at buoys S1 and E1, respectively. Data are taken at the surface (approximately 1.2 m) from 1 July to 1 October 2006 at S1, and from 1 November to 31 December 2006 at E1. The red, green, and black lines refer to observations, INT1 and INT3 results, respectively.

variable considered (either temperature or salinity). Observations show high-frequency oscillations captured by INT1 and not INT3. As a confirmation of the impact that tidal currents have on near bottom transports, a spectral analysis was carried out on near-bottom transports along- and across-shore at the E1 buoy, and these are presented in Figure 10. The model with tides is in very good agreement with the observations.

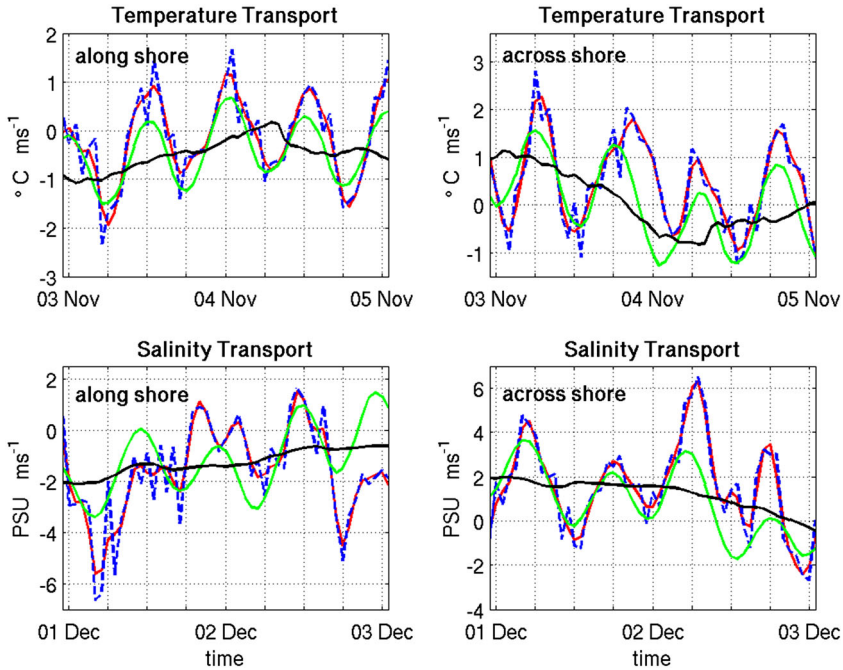

Figure 9. Modeled and observed near-bottom transports of temperature (top) and salinity (bottom) at buoy E1. Left- and right-hand panels refer to along-shore (positive toward north) and across-shore transports (positive toward open sea), respectively. The green and black lines are the estimates from INT1 and INT3 results. The blue dashed line is the transport estimated from observed raw data, while the red line is the transport estimated from observed data after the application of a filter allowing frequencies lower than 8 cpd.

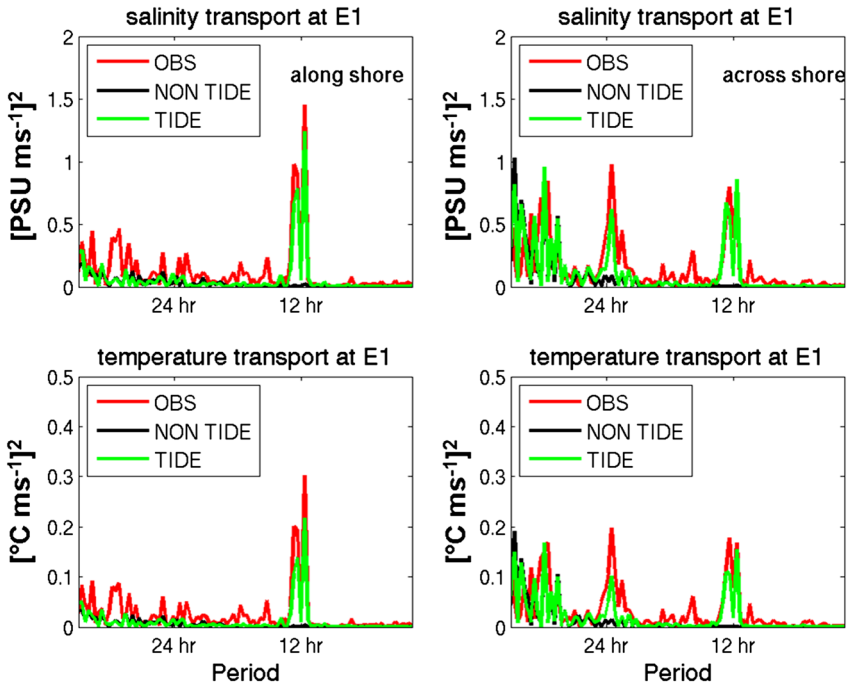

Figure 10. Power spectra of along and across-shore (left and right, respectively) bottom transport of salinity and temperature (top and bottom, respectively) at buoy E1.

[44] It is remarkable that semidiurnal tidal frequencies have the strongest impact in the along-shore transport, while the energy corresponding to the diurnal frequency is very low. For the cross-shore transport instead the diurnal frequencies are dominant, and the associated energy has the same order of magnitude as that associated with semidiurnal frequencies.

5.2. Effects of Tides on Mixing and Mean Circulation

[45] In ROFI regions stratification tends to be maintained by the continuous input of fresh water from the rivers, and is in competition with stirring activity due to the atmospheric forcings at the surface and friction at the bottom [*Simpson et al*., 1990]. In the presence of tides the vertical shear acts on the horizontal density gradients, inducing the lighter surface waters to move faster offshore above the heavier and more saline waters located in the lower layers, and contributing to add stability to the vertical structure [*Simpson et al*., 1990]. During ebb tides the currents, heading seaward, tend to take the surface lighter waters offshore, producing a higher stratification. On the contrary during floods the tidal component of the flow tends to bring the more saline waters from the open sea toward the coast, thus destroying the vertical structure formed during ebbs, resulting in a better-mixed water column. *Souza et al*. [2008] indicated that tidal-induced stratification can have ranges of up to 4 PSU in ROFI regions where the circulation is strongly tidally driven, such as the Rhine region (North Sea), and can cause complete water column mixing. This is not the case of the Adriatic, where tidal currents are one order of magnitude lower than in the North Sea, but we will show how this mechanism is sometimes appreciable.

[46] In Figure 11 an analysis of the difference between INT1 and INT3 results (tide-no tide) at the location of the buoy S1 is presented for all of February 2006 (Figure 11-1a) and August 2006 (Figure 11-1b). The mixed layer depth (MLD) has been calculated as the depth where the density difference with respect to the density at the surface exceeds 0.01 kg/m^3. The blue lines of Figures 11-1a and 11-1b represent the wind stress (Pa) at the air-sea interface and is labeled on the right y axis. Panels 2 to 6 represent the difference fields between INT1 and INT3 for temperature (°C), salinity (PSU), density (kg/m^3), cross-shore current shear (Pa) and vertical mixing coefficient for tracers (m^2/s) as defined in equations (A3) and (A4). The cross-shore current shear is $\mu(\partial u/\partial z)$, where z is the vertical direction, u the zonal velocity of the current, and μ is the dynamic viscosity of water (Nsm^{-2}). The black lines of panels 2 to 6 represent the difference of SSH between the results of INT1 and INT3.

[47] In winter the water column is generally well mixed, and the dynamics of the MLD is not greatly influenced by the presence of tides. The difference between the MLD with and without tides in Figure 11-1a is not large, except during high wind-stress periods. With tides and during strong wind-stress periods we have an evident enhancement of mixing. This is very much visible in Figure 11-6a between 4 and 7 February and in the last week of the same month, when the difference between the vertical mixing coefficients of INT1 and INT3 is very strong. Concomitantly the differences in temperature, salinity, and density are usually confined within 0.2°C, PSUs, and kgm^{-3}, respectively (3–7 and 23–24 of February). Only in the last two days of the month we have localized changes of salinity up to 1 PSU, and consequently of density. During the rest of the month, though, when wind stress is not as intense the vertical mixing coefficient difference between the two systems is not as important. Moreover, the intensity of the tidal-induced mixing is never enough to produce full mixing along the whole water column. This conclusion is also supported by Figure 12, where the INT1

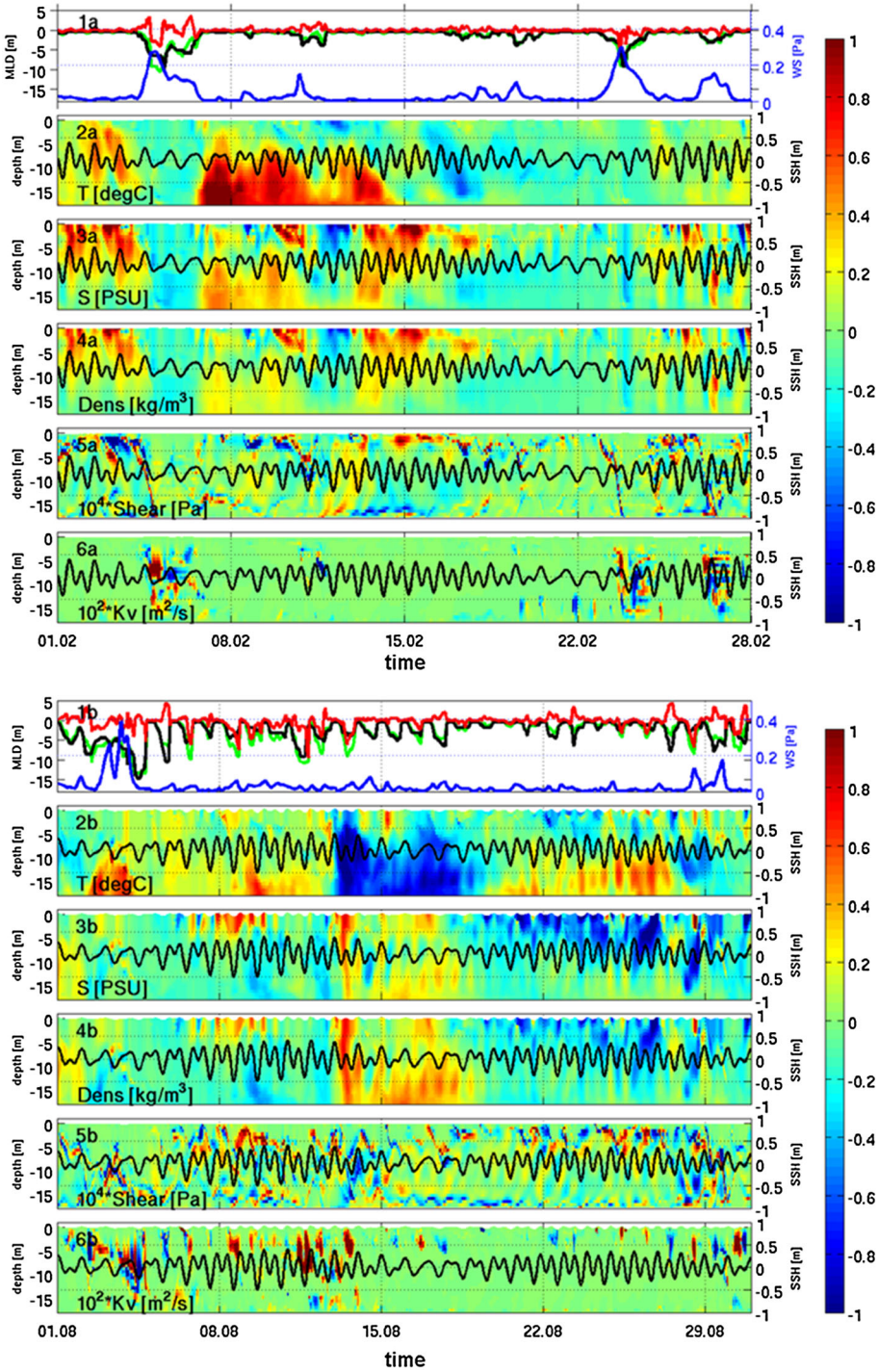

Figure 11. Analysis at S1 buoy location (lon=12.4575°E, lat=44.7424°N) of the difference between INT1 and INT3 results (Tide-NoTide), for the months of February (top) and August 2006 (bottom). In particular: 1 is tidal (green line) and nontidal (black line) mixed layer depth (meters), and their difference (meters, red line); wind stress (Pascal, blue line) at the air-sea interface; 2, 3, 4, 5, and 6 are the difference fields of temperature (°C), salinity (PSU), density (kg/m^3), zonal velocity shear (Pascal), and vertical eddy diffusivity (m^2/s) between INT1 and INT3 results. The black lines of panels 2 to 6 are the difference of SSH between the results of INT1 and INT3.

(green line) and INT3 (black line) modeled differences of salinity between the surface and the bottom at the location of buoy S1 are shown, together with the sea surface height of INT1 (blue dashed line, in meters) and the tidal component of the current (red dashed line, in dm/s) in the cross shore direction (i.e., along the *x*-axis), to evidence ebb and flood sea level and current cycles. The represented periods are 24–26 February 2006 (Figure 12, top) and 8–10 August

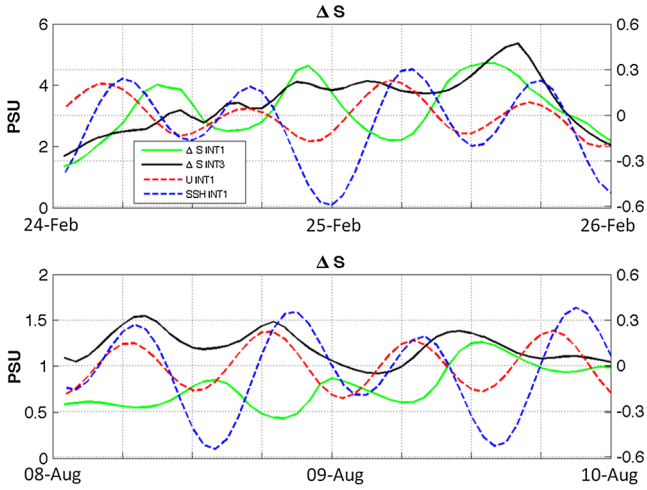

Figure 12. Bottom-to-surface salinity difference (ΔS expressed in PSU), sea surface height (SSH expressed in meters), and cross-shore tidal current component (expressed in dm/s) at buoy S1. The green and black lines represent ΔS for INT1 and INT3, respectively. The dashed blue line represents SSH in INT1. The red dashed line represents the cross-shore tidal current component (positive toward coast). Data are plotted on an hourly basis for the periods 24–26 February 2006 (top) and 8–10 August 2006 (bottom). ΔS is labeled on the left *y* axis; SSH and tidal current are labeled on the right *y* axis.

2006 (Figure 12, bottom). It is to be noted that the zonal component of the tidal current is positive when the flow is toward the coast and it is negative when the flow is seaward. During ebb tides the flow is seaward, inducing the lighter surface fresh water coming from the river to move faster offshore, thus contributing to add stability to the water column. This is clear in Figure 12 where the negative direction of the zonal current (ebb tide seawards) corresponds to increased stratification. The opposite process happens during flood tides, when the tidal component of the flow is toward the coast, inducing heavier water from the open sea to flow over the lighter coastal waters, thus adding instability to the water column and contributing to destroy stratification toward a mixed water column. This process is an example of the tidal mixing mechanism described by *Simpson et al*. [1990], and similar results related to a partial destratification of the water column due to tides in the northern Adriatic support previous findings by *Malačič et al*. [2000], but in this case a barotropic model was used. It is interesting to note that since in the Adriatic the tides have the character of standing waves, the flood current (maxima of the red dashed line of Figure 12) precede the high water, while the ebb current (minima of the red dashed line) precede the low waters. This is evident in Figure 12 as well, both for winter (upper panel) and summer (lower panel). This tidal induced mechanism of alternation of stratification and destratification is also clearly visible in Figures 11-3a and 11-4a during the last week of February, when the periodic vertical distribution of salinity and density is correlated to ebb and flood tidal cycles. The vertical distribution of temperature does not show tide-related fluctuations in winter.

[48] In summer the water column is stratified, and the diurnal cycle connected to the atmospheric forcing plays the chief role in the oscillation of the MLD. Tides, however, induce a different stratification along the water column, following the mechanism described above.

[49] As studies have recently shown, internal tides were evidenced in the southern [*Mihanović et al*., 2006] and middle [*Mihanović et al*., 2009] part of the Adriatic Sea basin. The semidiurnal oscillation of salinity visible during the days before and after 8 August (mainly in the upper layers), as well as during the whole second part of August (from the 20th to the end of the month, also in the lower layers; Figures 11-3b and 11-4b) demonstrates the presence of internal tides also in the northern part of the basin. Unlike with salinity, internal tide imprints on the temperature related to semidiurnal oscillations are only visible in summer (Figure 11-2b, last 10 days of August 2006).

[50] A further analysis of Figure 11 evidences how a very strong impact of tidal motion on the temperature and salinity tracers is due not just to tidal mixing, but also to different advection of water masses in the basin. As a matter of fact during certain periods of February and August differences in salinity and temperature are quite large, up to 1°C and 1 PSU respectively, in spite of small differences in mixing. This is the case of the middle two weeks of February and the last two of August. It evidences a strong component of the impact of tides on the horizontal advection, and not just on the vertical diffusion.

[51] This conclusion is also supported by Figure 13, which shows the mean circulation for August 2006 at 20 m (top panels) and at 100 m (bottom panels) simulated with INT1 (left panels) and INT3 (right panels). The red arrows and corresponding numbers in the figure highlight the main features and differences between the two systems, with and without tides. Because the only difference between the two integrations is the tidal forcing at the southern open boundary, we can assume that the resulting mean circulation differences are only related to tides. It is remarkable how the WACC changes in the area of the Promontory of Ancona, a zone of very high variability. In the model without tides the WACC (1) is located further offshore and a small anticyclone is formed between the current and the coast. In the model with tides the WACC (1) is much more constrained to the Promontory, and the anticyclone cannot form. This might be an effect of the nearby amphidromic node, and therefore related to the semidiurnal frequencies.

[52] Another difference in the circulation is in the region of the SAD, where a climatological cyclone is observed [*Artegiani et al*., 1997a, 1997b]. The tidal simulation shows a much larger cyclonic gyre (4) and a weaker anticyclonic area (5) than INT3. The variability of the currents 20 m deep along the coast of Puglia also changes significantly. In fact eddy (2) of INT1 is limited to the coast, while in INT3 it develops more offshore, and consequently shifts the southern part of the WACC (3) offshore.

[53] Besides the WACC, the other dominant feature of the circulation of this season is the middle Adriatic gyre. Its cyclonicity seems to be enhanced by the introduction of tides and its shape and intensity are better defined and marked in its northwest and southeast limits.

[54] The effect of tides is also evident in the circulation at depth, as shown in the bottom panels of Figure 13. Here the

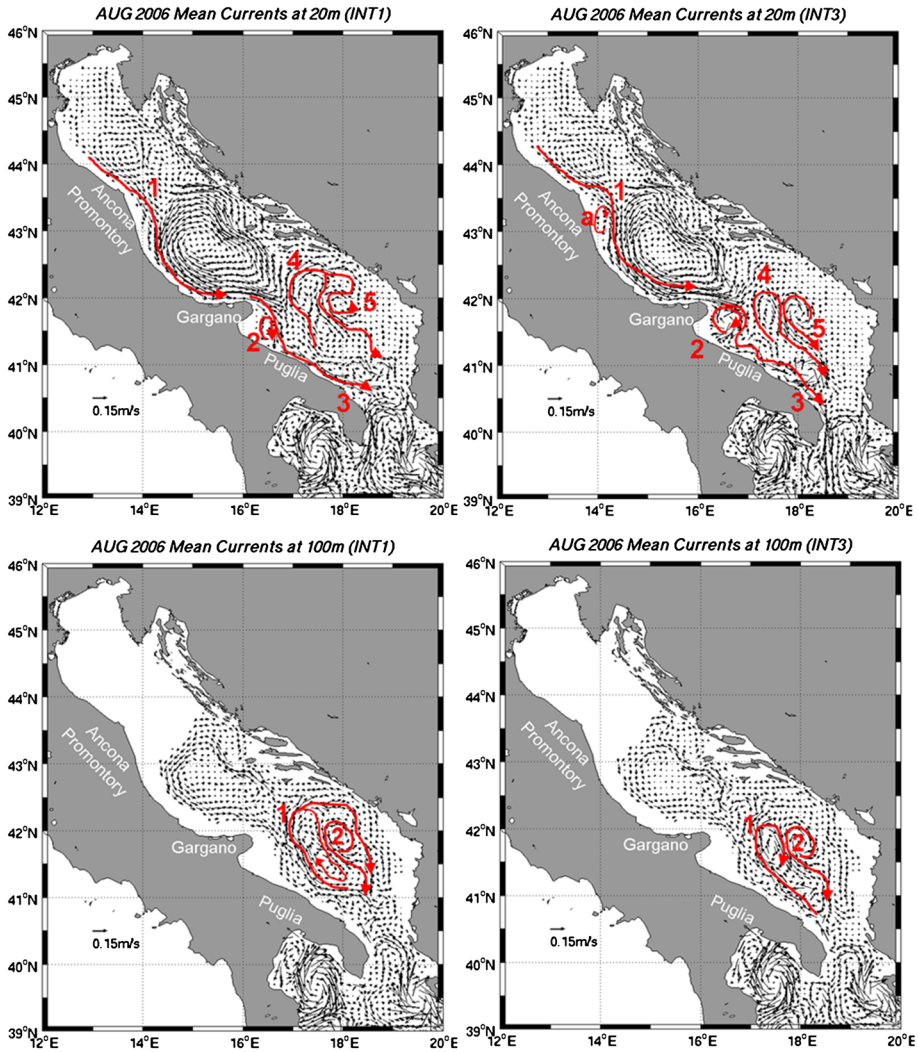

Figure 13. Mean currents of August 2006 at 20 m (top) and 100 m (bottom) for INT1 (left) and INT3 (right). The thick red arrows highlight the main features of the two systems and the differences between them.

cyclonic currents of the middle Adriatic are stronger in INT1 than in INT3. This may be due to an enhancement related to the Kelvin wave of the semidiurnal tidal constituents, which travels anticlockwise around the basin: going down the water column toward the bottom the nontidal component of the current weakens, so the tidal component, despite being moderate if compared to other seas where it may reach one order of magnitude higher, becomes proportionally more important.

[55] In the SAD region differences are also evidenced, very similarly to what happens in the same region at 20 m (see gyres 1 and 2).

6. Summary and Conclusions

[56] Tides were successfully introduced into a baroclinic primitive equation model of the entire Adriatic Sea. This was achieved through the implementation of a modified boundary condition at the southern boundary line [*Oddo and Pinardi*, 2008]. The impacts of tides on circulation characteristics were studied in the period 2000–2008.

[57] The main constituents of tides were analyzed in terms of tidal amplitude and phase, and the errors estimated versus the observed data were respectively 2% and 4% for the amplitude and phase of the most energetic constituents, the semidiurnal M2. A larger error was found for the diurnal tidal constituents, which are usually underestimated both in terms of amplitude (errors up to 25%) and phase (errors up to 10%). In general the errors on the phases were smaller than those on the amplitudes. These results show that the mean error in the main tidal harmonic constituents around the basin is comparable to that of barotropic tidal models [*Malačič et al.*, 2000; *Cushman-Roisin and Naimie*, 2002; *Bellafiore et al.*, 2008]. In addition, we have shown that the introduction of tidal barotropic velocity in the modified Flather boundary condition is important for the correct reproduction of tidal amplitude and phases, particularly for the diurnal constituents.

[58] The model was validated over a 9 year time period for currents, temperature, salinity, and sea surface elevation. The latter was analyzed at high frequency (1 h) for 8 tide-gauge stations around the basin, and the mean errors were

found to range between 6 and 9 cm, with an average value of approximately 7 cm. For temperature and salinity the highest errors averaged in space and time are evidenced in the upper part of the water column, confined within 1.5°C and 1.3 PSUs, respectively, and rapidly decreasing within the first 100 m of depth. The validation of the full coastal currents showed that the model is capable of reproducing them well, even though the highest and lowest peaks of intensity are often underestimated. The simulated tidal components of velocity fit the observations much better.

[59] The baroclinicity of the model allowed the study of the impact of tides on the dynamics of the system, as well as a detailed analysis of the processes affected by tides for different seasons of the year. The improvements due to the introduction of tides in the model and the impact on the system are significant, especially in the spectrum of high frequencies. In particular, in the ROFI region of the Po investigated here the transport of heat and salt was stronger along-shore than across-shore. In the alongshore direction the tidal transport is almost completely associated with semidiurnal frequencies, while in the cross-shore direction the transport related to diurnal frequencies also becomes important.

[60] In terms of stratification and mixing related to tides, we found that tide-induced mixing during flood currents is present in the ROFI region of the Po River due to the fact that the flood onshore currents tend to bring saltier waters over the coastal fresher waters, thus inducing destratification of the water column. This process is not powerful enough to induce a complete mixing of the water column as normally happens in the North Sea. Similar results on tidal induced mixing were also found in the northern Adriatic by *Malačič et al*. [2000] with a barotropic modeling approach. On the other hand, during ebb currents the tidal flow directed offshore tends to bring the river fresher waters seaward, inducing an enhancement of stratification. Moreover, clear oscillations of salinity and density along the water column were found in both winter and summer, while oscillations of temperature were only found in summer. These oscillations are an expression of internal tides in this specific area of the Adriatic Sea basin and this finding corroborates from a modeling point of view the previous empirical evidence of internal tides in different areas of the Adriatic [*Mihanović et al*., 2006, 2009].

[61] Another impact of tides on the physical system is that they influence not only the mixing, but also the circulation. They modify the horizontal advection, inducing a different momentum advective component in the basin, which in turn produces a different distribution of water masses in the basin. This happens more evidently in periods of weak wind stress. This finding is supported by the differences in the mean February and August circulation evidenced between INT1 and INT3 in Figure 13, and by the large differences in the temperature and salinity distributions in spite of the small differences in the vertical mixing coefficients (Figure 11).

[62] When the wind stress is stronger, the interaction between tides and vertical mixing also appeared to be strong. This is the first work to highlight this phenomenon, which has not yet been clarified regarding the details of the physical processes that drive it. This could be an interesting direction for future work, alongside studies of the oscillations of the thermocline due to tidal activity in the northern coastal areas of the Adriatic basin, and further investigations on internal tides in general. From the numerical point of view a great effort should definitely be made in the future to achieve an improvement in the reproduction of the diurnal constituent of tides.

Appendix A: Description of the Circulation Model Used

[63] The governing equations of the model are the equations of momentum and mass conservation ((A1) and (A2), respectively), of advection-diffusion of potential temperature θ and salinity S ((A3) and (A4) respectively), and the hydrostatic equation (A5)

$$\frac{\partial(u,v)}{\partial t} + U\cdot\nabla(u,v) + f(-v,u) = -\frac{1}{\rho_0}\left(\frac{\partial p}{\partial x},\frac{\partial p}{\partial y}\right) + \nabla_h \cdot(A_M\nabla(u,v)) + \frac{\partial}{\partial z}\left(K_M\frac{\partial(u,v)}{\partial z}\right), \tag{A1}$$

$$\nabla\cdot U = 0, \tag{A2}$$

$$\frac{\partial\theta}{\partial t} + U\cdot\nabla\theta = \nabla_h\cdot(A_v\nabla_h\theta) + \frac{\partial}{\partial z}\left(K_v\frac{\partial\theta}{\partial z}\right) + \frac{1}{\rho_0 c_p}\frac{\partial I}{\partial z}, \tag{A3}$$

$$\frac{\partial S}{\partial t} + U\cdot\nabla S = \nabla_h\cdot(A_v\nabla_h S) + \frac{\partial}{\partial z}\left(K_v\frac{\partial S}{\partial z}\right), \tag{A4}$$

$$\frac{\partial p}{\partial z} = \rho(S,\theta,p)g, \tag{A5}$$

where $U(u,v,w)$ is the velocity field in a local Cartesian coordinate system (x,y,z); p, g, ρ_0 are pressure, gravity, and a reference density value, respectively, f is the Coriolis parameter, A_{M} and A_{v} are the horizontal eddy viscosity and diffusion coefficients, while K_{M} and K_{v} are the vertical mixing coefficients for momentum and tracers respectively. Finally, c_{p} is the specific heat for water, and I is defined as $I(z)=Tr\,Q_{\mathrm{s}}e^{-\lambda z}$, where Tr is the coefficient of penetration of light into the water according to *Jerlov* [1976], Q_{s} the short-wave radiation incident to the sea surface, calculated through an astronomical formula according to *Reed* [1977] and described in *Chiggiato et al*. [2005] and *Maggiore et al*. [1998], and λ the absorption coefficient of light along the water column. The values for Tr and λ used were 0.31 and 0.042 m^{-1}, respectively.

[64] The density ρ is calculated according to the adaptation of the UNESCO formula proposed by *Mellor* [1991], the vertical mixing coefficients K_{M} and K_{v} are calculated with a second-order turbulence closure submodel [*Mellor and Yamada*, 1982], while the eddy viscosity is parameterized following the scheme of *Smagorinsky* [1993]. The background vertical eddy diffusivity is set to $2\cdot10^{-5}$ m^2/s.

[65] The advection terms in the hydrodynamics equations are solved with a Monotonic Up-Stream Scheme for Conservation Law [*Estubier and Lévy*, 2000], while the horizontal diffusive fluxes of temperature and salinity are calculated by subtracting the weekly mean fields from the instantaneous values.

[66] The model uses explicit time stepping for the free surface equation written integrating the continuity equation (A2)

vertically, and the time step is 4 s. The full baroclinic equation is solved with a time step of 400 s.

A1. Vertical Boundary Conditions

[67] The air-sea interaction is calculated through bulk formulae by means of the atmospheric forcings and of the sea surface temperature predicted by the model, and results in the following surface boundary conditions for heat (A6) and momentum (A7):

$$\rho_0 K_v \frac{\partial \theta}{\partial z}\Big|_{z=\eta} = \frac{1}{c_p}((1-Tr)Q_s - Q_B - Q_c - Q_h), \tag{A6}$$

$$\rho_0 K_M \frac{\partial (u,v)}{\partial z}\Big|_{z=\eta} = (\tau_x, , \tau_y), \tag{A7}$$

where η is the surface elevation, Q_{B} is the long wave radiation flux computed through the formula proposed by May (1986), while Q_{E} and Q_{h} are the latent and sensible heat fluxes respectively (computed according to Kondo, 1975); τ_x and τ_y are the zonal and meridional components of the wind stress produced on the sea surface, computed according to *Hellerman and Rosenstein* [1983].

[68] The atmospheric state variables used to compute the air-sea fluxes above are the analyses of the ECMWF at a horizontal resolution of 0.5°, available every 6 h.

[69] Regarding the surface boundary condition for the vertical velocity, a realistic freshwater balance is used according to (A8)

$$w\big|_{z=\eta} = \left(\frac{\partial \eta}{\partial t} + \vec{u}\cdot\nabla\eta\right)\Big|_{z=\eta} + (E - P - R/A), \tag{A8}$$

where E, P, and R are evaporation, precipitation and river runoff and A is the river cross-sectional area at the relevant grid cell chosen to the outflow. The normalized river runoff (R/A) of equations (A8) and (A9) is directly associated with the model grid point corresponding to the river's estuary [*Simoncelli et al*., 2011]. The rivers implemented and their relative positions are those described in *Zavatarelli and Pinardi* [2003] (Figure 1).

[70] The water balance (E-P-R/A) is also used to estimate the salinity flux at the surface according to (A9)

$$K_v \frac{\partial S}{\partial z}\Big|_{z=\eta} = S\big|_{z=\eta}(E - P - R/A). \tag{A9}$$

[71] The evaporation is calculated from the latent heat fluxes, while the precipitation comes from the climatological data set from *Legates and Willmott* [1990], and the fresh water runoff, except for the Po and Buna/Bojana, is taken from Raicich's climatology [*Raicich*, 1994]. The Po flow values used are daily means observed at the cross-section of Pontelagoscuro, a few dozen kilometer upstream from the delta (see the black triangle of Figure 1 labeled 'PLS'), provided by the Agenzia Regionale Prevenzione e Ambiente, Servizio Idro Meteo (ARPA-SIM) of the Emilia-Romagna region, while the *Raicich*'s [1994] Buna/Bojana climatological flow values have been substituted with those of *UNEP* [1996], recently investigated by *Marini et al*. [2010].

[72] At the bottom the vertical boundary condition for the continuity equation (A2) results in

$$w\big|_{z=-H} = -\left(u_b \frac{\partial H}{\partial x} + v_b \frac{\partial H}{\partial y}\right)_{z=-H}, \tag{A10}$$

where H is the water depth, and $\rightarrow u_b$ is the bottom or last level velocity, while the boundary condition for the momentum flux is:

$$\rho_0 K_M \left(\frac{\partial (u,v)}{\partial z}\right)_{z=-H} = (\tau_{bx}, \tau_{by}), \tag{A11}$$

where τ_{bx} and τ_{by} are the zonal and meridional components of the bottom stress

$$\vec{\tau}_b = C_d \rho |\vec{u}_b| \vec{u}_b, \tag{A12}$$

in which C_{d} is the bottom drag coefficient

$$C_d = \max\left\{0.0025; \left[\kappa / \ln\left(\frac{\delta_b}{z_0}\right)\right]^2\right\}, \tag{A13}$$

where κ is the Von Kármán constant (equal to 0.40), z_0 is the bottom roughness length scale, and δ_{b} the thickness of the last model level above the bottom.

[73] For tidal motion it is customary to use a calibration procedure to find the best value for the bottom drag coefficient in equations (A12) and (A13). Simulations have been performed with the simply barotropic model forced with tidal velocities and elevation at the open boundary line. This procedure was applied to the M2 and K1 constituents. The bottom roughness value that allowed reproduction of the barotropic amplitude literature results [*Malačič et al*., 2000; *Cushman-Roisin and Naimie*, 2002; *Bellafiore et al*., 2008] was found to be z_0 = 0.001 m. Some investigations have also been carried out with the depth-dependent bottom drag coefficient from the Gauckler-Strickler-Manning formula [*Gauckler*, 1867], but the results were not as satisfactory as those with the conventional quadratic drag coefficient.

[74] **Acknowledgments.** This work was funded by the Italian Ministry of Environment, Land and Sea through the Project ADRICOSM INTEGRATED RIVER BASIN AND COASTAL ZONE MANAGEMENT SYSTEM: Montenegro coaSTal ARea and Bojana river catchment (ADRICOSM-STAR), in the framework of the ADRICOSM-Partnership, and also supported by the European Commission MyOcean2 Project (SPA.2011.1.5-01) Prototype operational continuity of GMES services in the Marine Area. Part of the CTD data used were kindly provided by NURC (NATO Undersea Research Centre). The S1 and E1 Buoys are operated by ISMAR and have been supported by CNR, ARPA Emilia Romagna, and the EMME/LIFE and ADRICOSM Projects.

References

Artegiani, A., D. Bregant, E. Paschini, N. Pinardi, F. Raicich, and A. Russo (1997a), The Adriatic Sea general circulation. Part I: Air-sea interactions and water mass structure, *J. Phys. Oceanogr.*, *27*(8), 1492–1514.

Artegiani, A., D. Bregant, E. Paschini, N. Pinardi, F. Raicich, and A. Russo (1997b), The Adriatic Sea general circulation. Part II: Baroclinic circulation structure, *J. Phys. Oceanogr.*, *27*(8), 1515–1532.

Bellafiore, D., G. Umgiesser, and A. Cucco (2008), Modeling the water exchanges between the Venice Lagoon and the Adriatic Sea, *Ocean Dyn.*, doi:10.1007/s10236-008-0152-7.

Blumberg, A., and G. Mellor (1987), A description of a three-dimensional coastal ocean circulation model, in *Three-dimensional coastal ocean models*, edited by N. Heaps, p. 208, Washington, DC7 American Geophysical Union.

Book, J., H. Perkings, and M. Wimbush (2009), North Adriatic tides: observations, variational data assimilation modeling, and linear tide dynamics, *Geofizika*, *26*, 115–143.

Bortoluzzi, G., F. Frascari, P. Giordano, M. Ravaioli, G. Stanghellini, A. Coluccelli, G. Biasini, and A. Giordano (2006), The S1 Buoy station, Po River Delta: data handling and presentation, *Acta Adriatica*, *47*(Suppl.), 113–131.

Buljan, M., and M. Zore-Armanda (1976), Oceanographical properties of the Adriatic Sea, *Oceanogr. Mar. Biol. Ann. Rev.*, *14*, 11–98.

Cardin, V., and M. Gačić (2003), Long term heat flux variability and winter convection in the Adriatic Sea, *J. Geophys. Res.*, *108*(C9), 8103–8115, doi:10.1029/2002JC001645.

Changshui, X., Q. Fangli, Y. Yongzeng, M. Jian, and Y. Yeli (2006), Three-dimensional structure of the summertime circulation in the Yellow Sea from a wave-tide-circulation coupled model, *J. Geophys. Res.*, *111* (C11S03), doi:10.1029/2005JC003218.

Chiggiato, J., M. Zavatarelli, S. Castellari, and M. Deserti (2005), Inter-annual variability of surface heat fluxes in the Adriatic Sea in the period 1998-2001 and comparison with observations, *Science of the Total Environment*, *353*, 89–102.

Cushman-Roisin, B., and C. E. Naimie (2002), A 3D finite-element model of the Adriatic tides, *J. Mar. Systems*, *37*, 279–297.

Egbert, G., and S. Erofeeva (2002), Efficient inverse modeling of barotropic ocean tides, *J. Atmos. Oceanic Technol*, *19*(2), 183–204.

Estubier, A., and Lévy M. (2000), Quel schéma numérique pour le transport d'organismes biologiques par la circulation océanique. Note Techniquesdu Pôle de modélisation, Institut Pierre-Simon Laplace, 18pp.

Flather, R. A. (1976), A tidal model of the northwest European continental shelf, *Memories de la Societe Royale des Sciences de Liege*, *6*(10), 141–164.

Gauckler, P. (1867), Etudes Théoriques et Pratiques sur l'Ecoulement et le Mouvement des Eaux, Comptes Rendues de l'Académie des Sciences, pp. 818–822, Paris, France, Tome 64.

Guarnieri, A., P. Oddo, G. Bortoluzzi, M. Pastore, N. Pinardi, and M. Ravaioli (2010), The Adriatic Basin Forecasting System: new model and System development. Coastal to Global Operational Oceanography: Achievements and Challenges, in *Proceedings of the 5th International Conference on EuroGOOS*, edited by H. Dahlin, M. J. Bell, N. C. Flemming S. E. Petersson, pp. 184–190, Exeter, UK.

Hellerman, S., and M. Rosenstein (1983), Normal monthly wind stress over the world ocean with error estimates, *J. Phys. Oceanogr.*, *13*, 1093–1104.

Hendershott, M., and A. Speranza (1971), Co-oscillating tide in long, narrow bays: the Taylor problem revisited, *Deep Sea Research*, *18*, 959–980.

Jerlov, N. (1976), *Marine Optics*, Elsevier Sci. Pub. Co.

Kondo, J. (1975), Air-sea bulk transfer coefficients in diabatic conditions, *Boundary Layer Meteorol.*, *9*, 91–112.

Legates, D., and C. Willmott (1990), Mean seasonal and spatial variability in a gauge corrected global precipitation, *Int. J. Climatol.*, *10*(2), 111–127.

Maggiore, A., M. Zavatarelli, M. Angelucci, and N. Pinardi (1998), Surface heat and water fluxes in the Adriatic Sea: seasonal and interannual variability, *Phys. Chem. Earth*, *23*(5), 561–567.

Malačič, V., D. Viezzoli, and B. Cushman-Roisin (2000), Tidal dynamics in the northern Adriatic Sea, *J. Geophys. Res.*, *105*, 26,265–26,280.

Marini, M., F. Grilli, A. Guarnieri, B. H. Jones, Z. Kljajic, N. Pinardi, and M. Sanxhaku (2010), Is the southeastern Adriatic Sea coastal strip an eutrophic area?, *Est. Coast. Shelf Sc.*, *88*(3), 395–406.

May, P. W. (1986), A brief explanation of Mediterranean heat and momentum flux calculations, NORDA Code 322, *Nav Oceanogr Atmos Res Lab*, Stennis Space Center, Miss, *5* pp.

Mellor, G. (1991), An equation of state for numerical models of ocean and estuaries, *J. Atmos. Ocean Technol.*, *8*, 609–612.

Mellor, G. L., and T. Yamada (1982), Development of a turbulence closure model for geophysical fluid problems, *Rev. Geophys. Space Phys.*, *20*, 851–875.

Mihanović, H., M. Orlić, and Z. Pasarić (2006), Diurnal internal tides detected in the Adriatic, *Ann. Geophys.*, *24*, 2773–2780.

Mihanović, H., M. Orlić, and Z. Pasarić (2009), Diurnal thermocline oscillations driven by tidal flow around an island in the Middle Adriatic, *Journal of Marine Systems*, *78*, S157–S168.

Mosetti, F. (1987), Distribuzione delle maree nei mari italiani, *Boll. Oceanol. Teor. Appl.*, *5*, 65–72.

Mosetti, R. (1986), Determination of the current structure of the M2 tidal component in the northern Adriatic by applying the rotary analysis to the Taylor problem, *Boll. Oceanol. Teor. Appl.*, *IV*, 165–172.

Nash, J., and J. Sutcliffe (1970), River flow forecasting through conceptual models part I - A discussion of principies, *J. Hydrol.*, *10*(3), 282–290.

Oddo, P., and A. Guarnieri (2011), A Study of the Hydrographic Conditions in the Adriatic Sea from Numerical Modelling and Direct Observations (2000-2008), *Ocean Science*, *7*, 549–567.

Oddo, P., and N. Pinardi (2008), Lateral Open Boundary Conditions for Nested Limited Area Models: Process selective approach, *Ocean Modeling*, *20*(2), 134–156.

Oddo, P., N. Pinardi, and M. Zavatarelli (2005), A numerical study of the interannual variability of the Adriatic Sea (1999-2002), *Science of the Total Environment*, *353*, 39–56.

Oddo, P., N. Pinardi, M. Zavatarelli, and A. Coluccelli (2006), The adriatic basin forecasting system, *Acta Adriat.*, *47*(Suppl), 169–184.

Orlić, M., M. Gačić, and P. La Violette (1992), The currents and circulation of the Adriatic Sea, *Oceanol. Acta*, *15*(2), 109–124.

Orlić, M., M. Kuzmić, and Z. Pasarić (1994), Response of the Adriatic Sea to the bora and sirocco forcings, *Cont. Shelf Res.*, *14*(1), 91–116.

Orlić, M., V. Dadić, B. Grbec, N. Leder, A. Marki, F. Matić, H. Mihanović, G. Beg Paklar, M. Pasarić, Z. Pasarić, and I. Vilibić (2006), Wintertime buoyancy forcing, changing seawater properties, and two different circulation systems produced in the Adriatic, *J. Geophys. Res.*, *111*, C03S07, doi:10.1029/2005JC003271.

Orlić, M., G. Beg Paklar, V. Dadić, N. Leder, H. Mihanović, M. Pasarić, and Z. Pasarić (2011), Diurnal upwelling resonantly driven by sea breezes around an Adriatic island, *J. Geophys. Res.*, *116*, C09025, doi:10.1029/2011JC006955, 10 PP.

Pawlowicz, R., B. Beardsley, and S. Lentz (2002), Classical Tidal armonic Analysis Including Error Estimates in MATLAB using T_TIDE, *Computers and Geosciences*, *28*, 929–937.

Pettenuzzo, D., W. Large, and N. Pinardi (2010), On the corrections of ERA-40 surface flux products consistent with the Mediterranean heat and water budgets and the connection between basin surface total heat flux and NAO, *J. Geophys. Res.*, *115*, C06022, 15, doi:10.1029/2009JC005631.

Pinardi, N., and G. Coppini (2010), Operational oceanography in the Mediterranean Sea: the second stage of development, *Ocean Science*, *6*, 263–267.

Pinardi, N., I. Allen, E. Demirov, P. D. Mey, G. G. Korres, A. Lascaratos, P. Y. L. Traon, C. Maillard, G. Manzella, and C. Tziavos (2003), The mediterranean ocean forecasting system: first phase of implementation (1998-2001), *Ann. Geophys.*, *21*, 3–20.

Pinardi, N., E. Arneri, A. Crise, M. Ravaioli, and M. Zavatarelli (2006), The Physical, Sedimentary and Ecological Structure and Variability of Shelf Areas in the Mediterranean Sea, in *The Sea*, vol. *14*, edited by A. Robinson and K. Brink, pp. 1243–1330, Harvard University Press, Cambridge, USA.

Polli, S. (1960), La Propagazione delle Maree nell'Adriatico, in *Atti del IX Convegno dell' Associazione Geofisica Italiana*, p. 11, Associazione Geofisica Italiana, Roma.

Poulain, P. (2001), Adriatic Sea surface circulation as derived from drifter data between 1990 and 1999, *J. Mar. Syst.*, *29*, 3–32.

Poulain, P., E. Mauri, and L. Ursella (2004), Unusual upwelling event and current reversal off the Italian Adriatic coast in summer 2003, *Geophys. Res. Lett.*, *31*(L05303), doi:10.1029/2003GL019121.

Pullen, J., J. D. Doyle, T. Haack, C. Dorman, R. P. Signell, and C. M. Lee (2007), Bora event variability and the role of air-sea feedback, *J. Geophys. Res.*, *112*, C03S18, p. 17, doi:10.1029/2006JC003726.

Raicich, F. (1994), Note on the flow rates of the Adriatic rivers, Tech.report, CNR. Ist. Sper. Talassografico, Trieste, Italy.

Reed, R. (1977), On estimating insolation over the ocean, *J. Phys. Oceanogr.*, *7*(3), 482, doi:10.1175/1520-0485(1977)007<0482:OEIOTO>2.0.CO;2.

Russo, A., A. Coluccelli, I. Iermano, F. Falcieri, M. Ravaioli, G. Bortoluzzi, P. Focaccia, G. Stanghellini, C. R. Ferrari, J. Chiggiato, and M. Deserti (2009), An operational system for forecasting hypoxic events in the northern Adriatic Sea, *Geofizika*, *26*(2), 191–212.

Sanchez-Arcilla, A., and J. Simpson (2002), The narrow shelf concept: couplings and fluxes, *Continental Shelf Research*, *22*, 153–172.

Sciarra, R., E. Bohm, E. D'Acunzo, and R. Santoleri (2006), The large scale observing system component of ADRICOSM: the satellite system, *Acta Adriatica*, *47*(Suppl.), 51–64.

Simoncelli, S., N. Pinardi, P. Oddo, A. J. Mariano, G. Montanari, A. Rinaldi, and M. Deserti. September 2011. Coastal Rapid Environmental Assessment in the Northern Adriatic Sea. *Dyn. Atmos. Oceans 52*(1–2), 250–283

Simpson, J., J. Brown, J. Matthews, and G. Allen (1990), Tidal straining, density currents and stirring control of estuarine stratification, *Estuaries 13*(2), 125–132.

Smagorinsky, J. (1993), Some historical remarks on the use of nonlinear viscosities, in *Large eddy simulations of complex engineering and geophysical flows*, edited by B. Galperin, and S. Orszag, pp. 3–36, Cambridge Univ. Press, New York.

Souza, A., N. Fisher, J. Simpson, and M. Howarth (2008), Effects of tidal straining on the semidiurnal cycle of dissipation in the Rhine region of freshwater influence: Comparison of model and measurements, *J. Geophys. Res.*, *113*, C01011, doi:10.1029/2006JC004002.

Tonani, M., N. Pinardi, S. Dobricić, I. Pujol, and C. Fratianni (2008), A high-resolution free-surface model of the mediterranean sea, *Ocean Science*, *4*, 1–14.

Tsimplis, M., R. Proctor, and R. Flather (1995), A two-dimensional tidal model for the Mediterranean Sea, *J. Geophys. Res.*, *100*, 16,223–16,239.

Umgiesser, G., D. Canu, A. Cucco, and C. Solidoro (2004), A finite element model for the Venice Lagoon. Development, set up, calibration and validation, *J. Mar. Syst. 51*, 123–145.

UNEP (1996), Implications of Climate Change for the Albanian Coast, Mediterranean Action Plan, MAP Technical Reports Series No.98.

Xingang, L., Q. Fangli, X. Changshui, W. Guansuo, and Y. Yeli (2010), Upwelling and surface cold patches in the Yellow Sea in summer: Effects of tidal mixing on the vertical circulation, *Cont. Shelf Res.*, *30*, 620–632.

Zavatarelli, M., and N. Pinardi (2003), The Adriatic Sea modelling system: a nested approach, *Ann. Geophys.*, *21*, 345–364.

Zavatarelli, M., J. Baretta, J. Baretta-Bekker, and N. Pinardi (2000), The dynamics of the Adriatic Sea ecosystem. An idealized model study, *Deep-Sea Res. I*, *47*, 937–970.

Zavatarelli, M., N. Pinardi, V. Kourafalou, and A. Maggiore (2002), Diagnostic and prognostic model studies of the Adriatic Sea circulation Seasonal variability, *J Geophys. Res.*, *107*(C1), 2-1-2-20, doi:10.1029/2000JC000210.

Zore-Armanda, M. (1979), Physical characteristics of the sea-water in the region of the Island of Hvar, *Acta Biol.*, *8*, 65–78.